Journal of Geochemical Exploration 158 (2015) 112–121

Contents lists available at ScienceDirect

Journal of Geochemical Exploration

journal homepage: www.elsevier.com/locate/jgeoexp

Geochemical and isotopic characteristics of geothermal springs hosted by deep-seated faults in Dongguan Basin, Southern China

Xumei Mao [a,*], Yanxin Wang [a], Hongbin Zhan [b], Liang Feng [a]

[a] School of Environmental Studies, State Key Laboratory of Biogeology and Environmental Geology, China University of Geosciences, Wuhan 430074, China
[b] Department of Geology and Geophysics, Texas A&M University, College Station, TX 77843, USA

ARTICLE INFO

Article history:
Received 30 November 2014
Revised 12 June 2015
Accepted 14 July 2015
Available online 20 July 2015

Keywords:
Water geochemistry
H and O isotopes
Geothermometer
Thermal spring
Deep-seated fault

ABSTRACT

Chemical and isotopic compositions of thermal springs and non-thermal springs and well from Dongguan Basian of Southern China were measured and used to assess the mechanism of hydrothermal system hosted by deep-seated faults. Thermal springs had relatively higher temperatures and dissolved ion contents than non-thermal springs and wells, and were classified as water chemistry type of HCO_3-Na + K. The reservoir temperatures were determined with their chemical compositions, and 131.0 to 138.9 °C estimated by a quartz geothermometer after steam loss were regarded as the most suitable assessment. Inadequate equilibrium between water and rock interaction is mostly speculated and the mixing with shallow non-thermal groundwater probably has minor contribution to the thermal springs. Stable isotope compositions of thermal springs ranged from −45.1‰ to −40.8‰ for δD and from −7.2‰ to −6.9‰ for $\delta^{18}O$, respectively. These isotopic results were almost identical to those of non-thermal springs. All the thermal and non-thermal groundwater samples scattered around the meteoric water lines, thus indicating meteoric water origin without further influences of evaporation and groundwater–rock interaction. The similarity of thermal and non-thermal groundwater in chemical and isotopic compositions suggested that groundwater migrating and being heated very quickly in a relatively fast conductive fracture system hosted by deep-seated faults mostly represented the mechanism of thermal springs.

1. Introduction

Thermal springs are associated with various heat sources, such as active volcano (Fischer et al., 1997; Guido and Campbell, 2012; Ishikawa et al., 2007; Tassi et al., 2003; Werner et al., 2008), magma intrusion (Minissale et al., 2007), tectogenesis and radioactivity (Guo and Wang, 2012; Larson et al., 2009; Mottl et al., 2011; Zaher et al., 2012). The distribution of thermal springs depends on different tectonic backgrounds, such as extrusion, collision, subduction, faults and the edge of sedimentary basin (De Filippis and Billi, 2012; Han and Huh, 2009; Lau et al., 2008; Thiebaud et al., 2010; Ueda et al., 2006; Yokoyama et al., 1999). With respect to the form of thermal springs hosted by faults, it is generally considered to be the mixing of deep thermal water and shallow non-thermal groundwater (Capaccioni et al., 2011; Duchi et al., 1992; Majumdar et al., 2005; Minissale et al., 1997; Parry and Bowman, 1990; Ruffa et al., 1999). In southern China, a large number of thermal springs focus on the fault zones and are exposed into a linear distribution (Huang and Goff, 1986; Lin et al., 2010; Sun et al., 2006). Most of thermal springs had been used to warm water aquaculture and health bath, and recently raised much interest for potential development of geothermal exploitation for green energy. Despite this increasing interest, few works had been published on the chemistry and isotopes of these thermal springs in southern China because their recharge temperatures are generally less than 90 °C.

In the recent four years, we found that the subsurface temperatures of some thermal springs or boreholes (artesian and the depth no more than 600 m) are around 120 °C near Dongguan Basin, Southern China. These temperatures considered as hopeful power generation using thermal groundwater raised the concentrations of the economic use and the origin of water for thermal springs. Then heat sources and water circulation need further investigation as they are hosted by deep-seated faults in the non-magmatic activity area that is untypical for thermal springs with high temperature. Recently, the mechanisms of nearby submarine thermal springs had been outlined as well as the evolutions of local geology and geochemistry in Southern China (Guo et al., 2012; Liang et al., 2007; Lin et al., 2010; Ye et al., 2014). Although the thermal springs around Dongguan Basin are known and used since dozens of years, the origin and the structure of these hydrothermal systems are still not well understood. The main objective of this paper is therefore to characterize the thermal springs hosted by deep-seated faults in Dongguan Basin with the first set of geochemical data and water stable isotopes. Comparison with non-thermal groundwater (from non-thermal springs or wells) helps to understand the recharge sources and to outline the potential hydrothermal mechanisms.

* Corresponding author.
E-mail address: maoxumei@cug.edu.cn (X. Mao).

http://dx.doi.org/10.1016/j.gexplo.2015.07.008
0375-6742/

2. Hydrogeologic setting

Dongguan Basin is located in the east part of Pearl River Delta Regions, Guangdong province of Southern China (Fig. 1). The terrain is tilted from northeast to southwest. The southwest part, estuarine sedimentary plain with relatively flat topography, is about 10 m above mean sea level (m.s.l.). The northeast part, low mountains and hills, is about 100 m above m.s.l. It is a sub-tropical monsoon climate with an average annual temperature of 23.3 °C. The local annual precipitation is 1336 mm, while the annual evaporation is up to 1100 mm.

Three broad stages of regional geological activity (known as Sinian–Silurian, Devonian–Mid-Triassic, and Later Triassic–Present) had a great influence on the local strata and geology structure. As magma intrusion from Paleozoic to Mesozoic and the subduction of Pacific plate and Eurasian plate (Guo et al., 2012; Zhu et al., 2010), granite is the most widely outcropping bedrock, accounting for more than 40% of bedrocks at Guangdong province (Song et al., 2011). A series of complicated tectonic activities form the main deep-seated faults with the direction of northeast, accompanying with continuous stratigraphic deposition, which have undergone frequent metamorphism and intense magmatism (GBGMI, 1988). Two deep-seated faults existing in the studied area, F1 and F2 in Fig. 1, are known as Heyuan Fault and Zijin–Boluo Fault, respectively.

Four hydrostratigraphic groups can be recognized according to different types of lithology and pore structures in the studied area. The coarse-medium sands and gravel of Quaternary strata are rich in pore water as the first hydrostratigraphic group distributed in the delta plain, mountain basins and coastal plains. Local main hydrostratigraphic group (the second group), are red sandstones and siltstones of Jurassic to Tertiary strata with abundant fissure water, which are widely distributed in the studied area and up to 1500 m of sedimentary thickness in Dongguan Basin. The limestone fissure water mainly exists in Carboniferous to Permian strata as the third hydrostratigraphic group

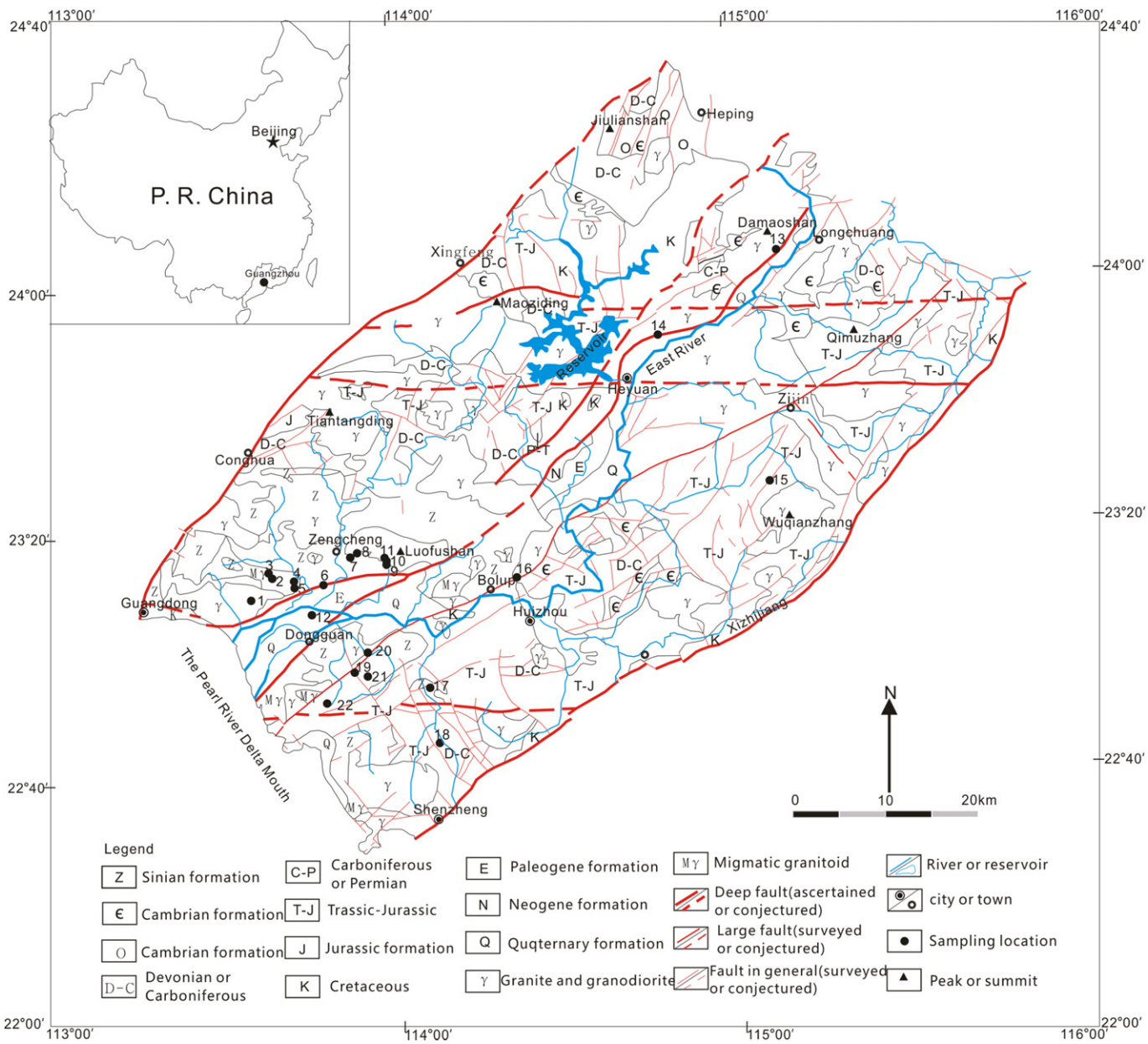

Fig. 1. Simplified map of geology and tectonic structure of Dongguan Basin and its surrounding areas in Guangdong province of Southern China. F1 and F2 represent Heyuan Fault and Zijin–Boluo Fault, respectively.

distributed in the edge of Dongguan Basin. The last hydrostratigraphic group is rich in fissure water in the fault zone of granite and tuff, which contain abundant groundwater with a non-uniform spatial distribution pattern.

Groundwater recharge was generally considered from atmospheric precipitation and the leakage of water from the local river. Groundwater flows from northeast to southwest along the main flow path and eventually discharges to the Pearl River. Along the fault belts of Heyuan and Zijin–Boluo (F1 and F2), groundwater is abundant and thermal springs emerge occasionally. Their appearance was speculated partly as the result of cooling process of magma intrusion in Southern China, partly as the mixture of deep geothermal fluid communicated by deep-seated faults (Zhou et al., 2009).

3. Sampling and analysis methods

Water samples were collected from springs and wells as well as from surface water in Dongguan Basin and surrounding area for chemical and isotope analyses (see sampling sites in Fig. 1). The groundwater collected from wells is different in depth. Sampling was carried out close to the well heads. Prior to sample collection, well water had been pumped until the conductivity reached to a stable value.

Four artesian thermal springs were sampled. Two of them (DG-13 and DG-14) are located at F1, one (DG-16) appears at F2, and the fourth (DG-15) exists at a small fault which is close and parallel to F2. In addition, six non-thermal artesian springs and ten drinking water wells for local residents with depths less than 10 m were studied for the purpose of comparison. One borehole (DG-12) with the depth of 200 m was pumped to get water sample. Although the depth of groundwater table is only 4 m, salty groundwater was found in the borehole because the existence of a salt–gypsum layer with 30 m thickness. River water (DG-11) and rain water were also collected at the same time. The sampling locations and information were listed in Table 1.

The temperatures, electrical conductivity (EC), dissolved oxygen (DO) and pH values of water samples were measured in situ by the 5-Star multi-parameter water quality analyzer (520M-01 model). The alkalinity of samples was determined by titration in situ with 0.1 N HCl using methyl orange as indicator and the precision did not exceed ± 0.5 mg/L.

Water samples collected for geochemical analyses were filtered through 0.45 μm membranes in the field and subsequently separated in different aliquots. After rinsing several times with the sampled solution, water samples were stored in cleaned polyethylene (HDPE) bottles. One vial was unacidified sample for anion analyses and another vial was acidified with ultrapure nitric acid to pH < 2 for major cations analyses. Samples for stable isotopes analyses (δD and $\delta^{18}O$) were collected in HDPE bottles with no headspace and sealed tightly.

Major anions were determined using ion chromatograph (Dionex ICS1100) and major cations were analyzed using inductively coupled plasma optical emission spectrometry (ICP-OES, Perkin Elmer Icap 6300). The precision of anion and cation based on replicate analyses was ±2%. Measurements of hydrogen and oxygen rations in water samples were carried out by stable isotope ratio mass spectrometer (Thermo-Finnigan MAT253). Results were reported in the delta (δ) notation versus the SMOW standard and expressed in per-mille (‰). The precisions were better than ±1‰ and ±0.2‰ for δD and $\delta^{18}O$, respectively. All of the analysis works were done in the State Key Laboratory of Biogeology and Environmental Geology, China University of Geosciences (Wuhan).

Mineral saturation indices were calculated using PHREEQC version 3 (Parkhurst, and Appelo, 2013) for both thermal springs and non-thermal water.

4. Results

4.1. Hydrogeochemistry of thermal and non-thermal groundwater

The discharge temperatures of geothermal water varied from 59.8 to 78.6 °C, while those of non-thermal springs were relatively stable changing from 22.2 to 28.4 °C (Table 1). The thermal springs showed weak alkaline as pH > 7, and the spring DG-15 was up to 8.12. The non-thermal groundwater from most of springs and wells was characterized by low pH, and the well DG-06 was low to 5.52. Electric conductivity (EC) of all groundwater samples changed from 37 to 667 μs/cm, except the borehole DG-12 whose EC was up to 26.17 ms/cm because of a salt–gypsum layer of 30 m thick. EC seemed closely related to the temperature, because those of thermal springs were 563 to 667 μs/cm, but no more than 320 μs/cm in non-thermal springs and wells. Dissolved oxygen (DO) was generally lower in thermal springs than in the non-thermal springs and wells, probably because DO was consumed in the process of groundwater–rock interaction at high temperatures in the thermal springs, also probably because the non-thermal springs and wells were recharged with shallow groundwater rich in atmospheric oxygen.

Table 1
Background information of thermal and non-thermal springs from Dongguan Basin of Southern China.

No.	Sample	Latitude	Longitude	Description	Depth (m)	Temperature (°C)	Water[a]
1	DG-01	N23°09′13.5″	E113°34′36.8″	Well	10	24.8	Non-thermal groundwater
2	DG-02	N23°12′40.2″	E113°38′45.3″	Spring	Artesian	24.4	Non-thermal groundwater
3	DG-03	N23°13′21.6″	E113°38′12.4″	Spring	Artesian	24.0	Non-thermal groundwater
4	DG-04	N23°11′62.0″	E113°42′23.4″	Well	12	24.1	Non-thermal groundwater
5	DG-05	N23°11′06.0″	E113°42′30.7″	Well	7	25.2	Non-thermal groundwater
6	DG-06	N23°11′43.1″	E113°47′27.8″	Well	10	25.7	Non-thermal groundwater
7	DG-07	N23°16′09.1″	E113°52′07.9″	Spring	Artesian	24.2	Non-thermal groundwater
8	DG-08	N23°16′30.1″	E113°53′28.8″	Well	8	25.4	Non-thermal groundwater
9	DG-09	N23°14′31.9″	E113°58′41.2″	Well	9	25.4	Non-thermal groundwater
10	DG-10	N23°15′35.6″	E113°58′10.7″	Spring	Artesian	22.2	Non-thermal groundwater
11	DG-11	N23°15′12.8″	E113°58′24.7″	River	Artesian	24.1	Surface water
12	DG-12	N23°06′37.4″	E113°45′16.4″	Borehole	200	26.8	Non-thermal groundwater
13	DG-13	N24°04′29.6″	E115°08′59.4″	Spring	Artesian	63.2	Thermal groundwater
14	DG-14	N23°51′11.2″	E114°47′29.4″	Spring	Artesian	56.7	Thermal groundwater
15	DG-15	N23°26′49.6″	E115°06′26.9″	Spring	Artesian	78.6	Thermal groundwater
16	DG-16	N23°12′10.5″	E114°21′31.3″	Spring	Artesian	59.8	Thermal groundwater
17	DG-17	N22°54′25.2″	E114°05′52.6″	Well	100	24.8	Non-thermal groundwater
18	DG-18	N22°45′20.6″	E114°07′14.3″	Well	6	24.2	Non-thermal groundwater
19	DG-19	N22°57′09.1″	E113°52′26.5″	Spring	Artesian	25.7	Non-thermal groundwater
20	DG-20	N23°00′19.2″	E113°54′50.6″	Well	7	28.4	Non-thermal groundwater
21	DG-21	N22°56′30.4″	E113°54′50.6″	Well	5	25.4	Non-thermal groundwater
22	DG-22	N22°52′05.1″	E113°47′44.0″	Spring	Artesian	23.0	Non-thermal groundwater

[a] The temperatures of non-thermal groundwater depend on the ambient temperature and the groundwater temperatures more than 35 °C are considered as thermal groundwater.

Table 2
Hydrogeochemistry and isotopic compositions of H and O in thermal and non-thermal springs from Dongguan Basin of Southern China.

No.	Sample	Water	pH	EC (μs/cm)	DO (mg/L)	CO_3^{2-} (mg/L)	HCO_3^- (mg/L)	F^- (mg/L)	Cl^- (mg/L)	NO_3^- (mg/L)	SO_4^{2-} (mg/L)	Ca^{2+} (mg/L)	K^+ (mg/L)	Mg^{2+} (mg/L)	Na^+ (mg/L)	Dissolved SiO_2 (mg/L)	δD_{SMOW} (‰)	$\delta^{18}O_{SMOW}$ (‰)
1	DG-01	Well	9.80	223	11.51	29.2	5.3	0.91	14.56	3.53	22.34	19.67	11.62	3.05	13.98	23.38	−42.4	−6.6
2	DG-02	Spring	5.78	106	8.85	–	7.9	0.18	7.06	10.24	4.52	7.17	4.26	1.43	7.28	23.62	−43.4	−7.0
3	DG-03	Spring	7.60	44	6.20	–	25.7	0.23	5.48	1.15	6.70	2.05	0.76	0.46	5.33	27.11	−40.9	−6.8
4	DG-04	Well	6.20	150	4.79	–	40.9	0.64	11.63	9.06	5.51	12.01	4.73	1.52	10.46	25.76	−42.9	−6.6
5	DG-05	Well	6.07	316	2.64	–	45.5	0.20	40.95	17.28	16.04	25.25	18.91	3.01	27.36	26.25	−39.0	−6.2
6	DG-06	Well	5.52	312	2.66	–	24.4	0.41	34.21	19.73	12.89	17.77	14.11	3.18	24.87	13.09	−35.5	−5.9
7	DG-07	Spring	6.69	75	7.53	–	16.8	0.25	11.17	0.38	6.59	31.18	4.76	10.95	10.85	21.65	−40.5	−6.2
8	DG-08	Well	6.03	75	7.48	–	40.9	–	15.24	1.40	5.08	10.47	0.96	0.69	7.14	7.77	−44.3	−6.7
9	DG-09	Well	5.87	234	4.26	–	36.9	0.71	17.88	5.46	6.35	13.19	2.80	3.31	10.48	22.48	−37.9	−6.1
10	DG-10	Spring	6.11	37	7.53	–	31.6	0.17	5.00	0.37	3.46	2.09	1.74	0.73	3.81	24.71	−46.2	−7.2
11	DG-11	River	7.02	37	9.32	–	25.9	0.34	6.16	1.20	5.31	2.62	1.97	0.55	3.12	17.14	−43.2	−6.9
12	DG-12	Borehole	7.30	26,170	5.71	–	131.5	–	9766.15	56.69	1288.25	1061.00	163.10	520.10	4449.00	23.58	−20.4	−3.2
13	DG-13	Thermal spring	7.04	563	5.38	–	287.8	9.12	9.68	0.26	24.92	22.52	5.90	0.82	101.10	96.34	−44.2	−6.9
14	DG-14	Thermal spring	7.20	667	0.95	–	246.0	9.99	17.81	0.94	77.51	22.39	5.94	0.64	123.60	106.88	−40.8	−6.9
15	DG-15	Thermal spring	8.12	566	1.15	12.9	225.0	15.26	16.63	0.88	13.72	2.74	5.84	0.19	113.30	96.34	−45.1	−7.2
16	DG-16	Thermal spring	7.55	636	1.81	–	282.6	14.51	16.26	0.37	37.46	12.46	6.29	0.38	129.30	113.77	−44.0	−7.1
17	DG-17	Well	7.24	288	1.70	–	186.4	2.28	6.64	0.26	6.89	50.51	3.35	1.49	11.91	59.93	−43.5	−6.7
18	DG-18	Well	5.95	211	3.18	–	35.3	0.40	18.73	12.67	7.67	20.31	2.50	5.09	8.73	18.22	−41.7	−6.6
19	DG-19	Spring	6.71	104	7.08	–	44.5	0.24	6.98	2.15	7.29	10.69	1.91	1.91	3.92	15.78	−42.0	−6.5
20	DG-20	Well	7.04	660	4.76	–	259.0	0.62	39.00	0.31	89.37	87.88	21.92	7.10	35.56	19.22	−39.1	−5.9
21	DG-21	Well	5.79	676	1.55	–	54.9	0.23	16.45	55.63	33.60	35.75	22.29	5.91	62.48	15.99	−39.3	−6.0
22	DG-22	Spring	6.24	40	9.15	–	28.8	0.16	5.70	0.69	4.32	1.36	1.97	1.03	3.17	23.21	−43.9	−6.9
23		Rain	/	/	/	/	/	/	/	/	/	/	/	/	/	/	−60.1	−8.4

–, not detected.
/, not measured.

HCO_3^- was the main anion in all groundwater samples, with additional amount of Cl^- and SO_4^{2-} also detected in non-thermal springs and wells (Table 2). Na^+ and K^+ were the main cations in all groundwater samples, and a considerable content of Ca^{2+} also existed in non-thermal springs and wells. Based on the major element composition, the water chemistry type of thermal springs was classified as HCO_3-Na + K, but those of non-thermal springs and wells were from HCO_3-Na + K + Ca to HCO_3 + Cl-Na + K + Ca (Fig. 2). Unique Cl-Na type water only existed in borehole DG-12.

The dissolved silica content of thermal springs ranged from 96.34 to 113.77 mg/L, but from 7.77 to 27.11 mg/L in non-thermal springs and wells, except a slightly high content up to 59.93 mg/L in non-thermal spring DG-17 (Table 2).

4.2. Hydrogen and oxygen isotopes

The isotopic compositions of H and O of thermal springs varied from −45.1‰ to −40.8‰ and from −7.2‰ to −6.9‰, respectively (Table 2). Those of non-thermal springs and wells changed from −46.2‰ to −35.5‰ and from −7.2‰ to −5.9‰, respectively. Both thermal springs and non-thermal springs and wells have almost uniform average values of isotopic compositions, and the average values are very close to those of river (δD and $\delta^{18}O$ were −43.2‰ and −6.9‰, respectively), which probably suggests that the groundwater of all springs and wells has the same source as the river water.

5. Discussion

5.1. Hydrogeochemical thermometry

Various geothermometers had been introduced to calculate the reservoir temperature of geothermal groundwater based on the chemical compositions for decades (Arnórsson, 1985; Ben Dhia and Meddeb, 1990; Fournier and Truesdell, 1970; Minissale et al., 2003; Pauwels et al., 1993; Pope et al., 1987; Spycher et al., 2014). The most common silica (quartz, chalcedony, amorphous silica etc.) and alkali (Na–K, Na–K–Ca, Na–K–Ca–Mg etc.) geothermometry equations were derived from the equilibrium constants of specific mineral and solution reactions in geothermal reservoir based on empirical and semi-empirical laws. Each geothermometer has its applicable condition, for example, silica-based geothermometers were widely applied to calculate the temperature of low enthalpy reservoirs (Dulanya et al., 2010; Fournier and Truesdell, 1970; Pope et al., 1987; Verma, 2000, 2008); Na–K geothermometer was more suitable to estimate the reservoir temperatures above 180 °C (Arnórsson, 1985; Arnórsson et al., 1983); while Na–K–Ca geothermometer was more suitable for geothermal groundwater with high Ca contents (Fournier and Potter Ii, 1979; Fournier and Truesdell, 1973; Pope et al., 1987). The thermal springs in Dongguan Basin were HCO_3-Na + K types and contained a certain amount of dissolved SiO_2. The reservoir temperatures were evaluated by alkali (Na–K, Na–K–Ca–Mg) and silica (conductive cooling, maximum steam loss and chalcedony) geothermometer (Table 3).

The geothermometer calculation of each thermal spring yielded a wide range of reservoir temperatures, partly due to the errors in the coefficient of geothermometer equations (Du et al., 2005; Dulanya et al., 2010; Pope et al., 1987). For the same thermal spring, the highest reservoir temperatures were derived from the quartz geothermometer of silica-quartz conductive cooling (Fournier, 1977), which ranged from 160.4 to 170.4 °C for the four thermal springs; but the lowest reservoir temperatures were estimated by chalcedony geothermometer (Fournier, 1977), which ranged from 84.5 to 94.0 °C. The Na–K–Ca–Mg geothermometer (Giggenbach, 1988) proposed the reservoir temperatures ranging from 112.0 to 135.2 °C, which is close to the assessment of chalcedony geothermometer based on field study (Arnórsson et al.,

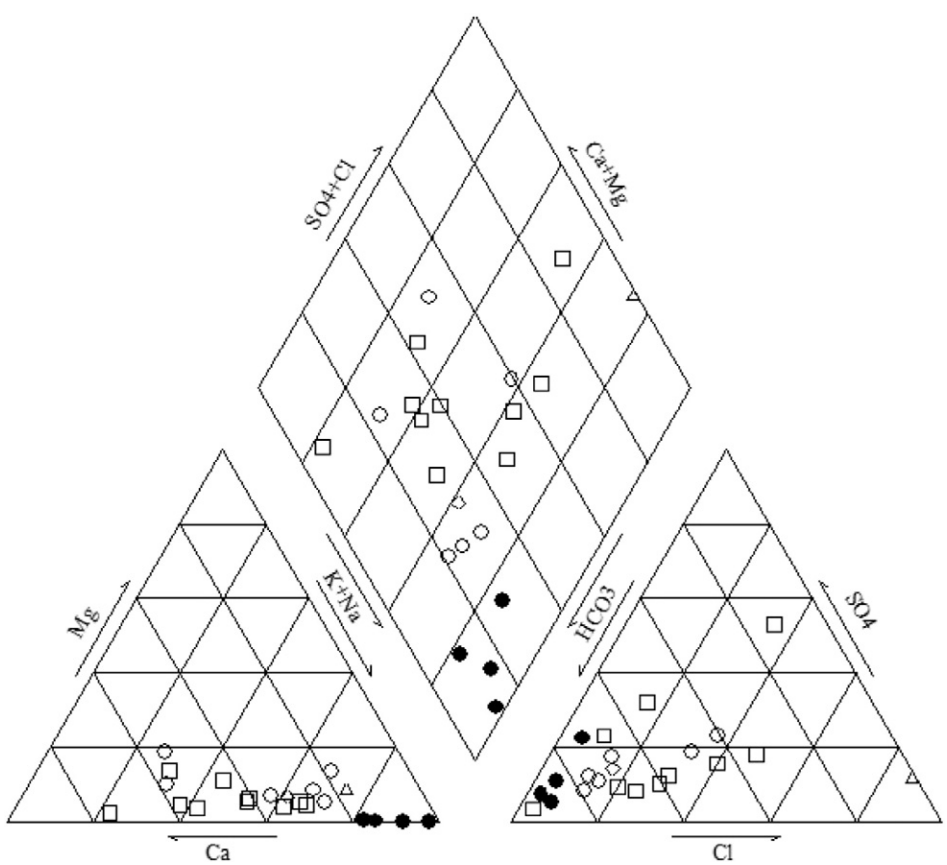

Fig. 2. Piper diagram for all water samples from Dongguan Basin and its surrounding areas in Guangdong province of Southern China. The dots represent the thermal springs, the circles represent the non-thermal spring, the squares the represent wells, the triangle represents the borehole DG-12, and the prismatic represents the river water.

Table 3
Temperature calculations with geothermometer using silica content and major cations of thermal springs from Dongguan Basin of Southern China.

Geothermometer (°C)		DG-13	DG-14	DG-15	DG-16
$T_{Na-K-Ca-Mg}$		112.0	112.9	135.2	119.5
T_{Na-K}		145.9	130.5	135.9	131.4
T_{SiO_2}	T1	160.4	166.6	160.4	170.4
	T2	131.0	135.9	131.0	138.9
	T3	84.5	90.3	84.5	94.0
	T4	106.9	112.8	106.9	116.5
	T5	136.8	142.9	136.8	146.8
	Arithmetic mean of SiO_2-based temperature	123.9	129.7	123.9	133.3

$T_{Na-K-Ca-Mg} = \frac{14920}{3\log[Na]/[K]+3\log([Ca]/[Na]^2)-\log([Mg]/[Na])+40.91} - 273.15$ (Giggenbach, 1988), where [Na], [K], [Ca] and [Mg] represent the concentrations of Na, K, Ca and Mg in mg/L, respectively.
$T_{Na-K} = \frac{933}{0.993+6\log([Na]/[K])} - 273.15$ (Arnórsson et al., 1983), where [Na] and [K] represent the concentrations of Na and K in mg/L, respectively.
T1 represents the temperature estimated by the quartz geothermometer of silica-quartz conductive cooling (Fournier, 1977): $t = 1390 / (5.19 - \log S) - 273.15$, where S is the aqueous SiO_2 in mg/L.
T2 represents the temperature estimated by the quartz geothermometer after steam loss (Fournier, 1977): $t = 1522/(5.75 - \log S) - 273.15$, where S is the aqueous SiO_2 in mg/L.
T3 represents the temperature estimated by the chalcedony geothermometer (Fournier, 1977): $t = 1000 / (4.78 - \log S) - 273.15$, where S is the aqueous SiO_2 in mg/L.
T4 represents the temperature estimated by the chalcedony geothermometer based on field study (Arnórsson et al., 1983): $t = 1112 / (4.91 - \log S) - 273.15$, where S is the aqueous SiO_2 in mg/L.
T5 represents the temperature estimated by the modified silica geothermometer (Verma and Santoyo, 1997): $t = -44.119 + 0.24469S - 1.7414 \times 10^{-4} + 79.305\log S$, where S is the aqueous SiO_2 in mg/L and less than 295 mg/L.

1983). While the Na–K geothermometer (Arnórsson et al., 1983) gave relatively high reservoir temperatures from 130.5 to 145.9 °C, and the similar reservoir temperatures were estimated by the modified silica geothermometer (Verma and Santoyo, 1997).

However, the ascent of geothermal waters from deep geothermal reservoir to the surface, they may be cooled by conductive heat loss as they travel through cooler rocks or by boiling due to decreasing hydrostatic head, and may be also diluted by shallow non-thermal groundwater to change the temperature and chemistry. Chemical geothermometers are based on temperature dependent water–rock equilibria and give the last temperature of water–rock equilibrium. The arithmetic mean of SiO_2-based temperatures are approximately equal to the cation geothermometer temperatures ($T_{Na-K-Ca-Mg}$ and T_{Na-K}), and much higher than the discharge temperatures of four thermal springs (Fig. 3). Then, this request that the chemical influence on SiO_2 and main cation can be ignore or consistent during the ascent of geothermal waters from deep geothermal reservoir to the surface. The

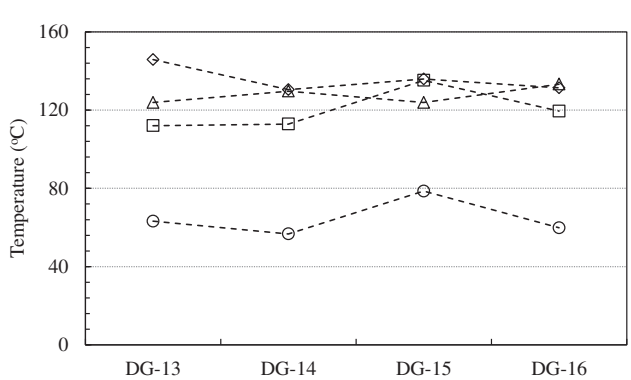

Fig. 3. Comparison of discharge temperatures and geothermometer calculated temperatures for the thermal springs. The dots represent the discharge temperatures measured in situ; the squares, diamonds and triangles represent the $T_{Na-K-Ca-Mg}$ (Giggenbach, 1988) and T_{Na-K} (Arnórsson et al., 1983), the arithmetic mean of SiO_2-based temperatures listed in Table 3, respectively.

four thermal springs have much higher Na and SiO_2 content but lower Mg content then non-thermal groundwater (Table 2). If thermal water mixing with a certain amount of non-thermal water, the Mg content in thermal springs should be higher than the non-thermal groundwater for the thermal groundwater should have highest Mg at higher temperature. Then SiO_2 geothermometer should be much different to cation geothermometer for the four thermal springs. So the mixing with shallow non-thermal groundwater probably has minor contribution to the four thermal springs. Furthermore, the variation of discharge temperatures of four thermal springs is similar to that of $T_{Na-K-Ca-Mg}$ in Fig. 3, probably resulting from the same cooled process by conductive heat loss. Therefore, the similarity of SiO_2-based temperatures and the cation geothermometer temperatures mostly indicates the lack of adequate equilibration in water–rock interaction at high temperature.

In comparison, the reservoir temperatures of four thermal springs estimated by the quartz geothermometer after steam loss (Fournier, 1977) have an approximation to the arithmetic mean of SiO_2-based temperatures (123.9 to 133.3 °C), and possibly represent the real geothermal temperature in the underground reservoir (131.0 to 138.9 °C). This speculation was based on that the thermal springs came from granite intrusion hosted by deep-seated faults, and that there were no observation in geothermal wells more than 120 °C in Dongguan Basin and surrounding area according to actual field investigation and literature record. Granite minerals provided the dissolved SiO_2 and deep-seated faults leaded to steam loss for the thermal springs. No more than 120 °C was observed in surface and subsurface indicating low-medium geothermal background.

Lack of a full chemical equilibrium in the thermal reservoir may cause the chemical geothermometers to provide uncertain results. One of the requirements for the successful application of cation geothermometers is the attainment of water–rock equilibrium in the geothermal reservoir. Due to re-equilibration degrees different to silica, the Na–K–Mg geothermometer were not considered reliable (Giggenbach, 1988; Shevenell and Goff, 1995). This consideration was evidenced from the distribution of thermal springs in the modified Na/400–K/100–$Mg^{1/2}$ (in mg/L) ternary diagram (Fig. 4). The four thermal springs were exclusively located in immature waters area and far away from the equilibrium line indicating the disequilibrium of groundwater and host rocks interaction. Their K–Mg apparent temperatures were less than 120 °C, but the K–Na apparent temperatures were greater than 280 °C. Moreover, the four thermal springs stay in the partial equilibrium line in the plot of $10C_{Mg}/(10C_{Mg} + C_{Ca})$ versus $10C_K/(10C_K + C_{Ca})$ as well as be close to the full equilibrium line (Fig. 5). According to Figs. 4 and 5, the studied thermal waters represent the immature waters that are not fully equilibrated with reservoir rocks. It seems that silica geothermometers may provide more reliable results than cation geothermometers because of the nonequilibrium conditions.

Based on the relation of dissolved silica and K–Mg contents, the full equilibrium lines were defined by plotting the logarithms of silica content versus K^2/Mg to estimate the reservoir temperatures (Giggenbach, 1988; Giggenbach and Glovert, 1992). In Fig. 6, the four thermal springs from Dongguan Basin showed lower reservoir temperatures of 85.6–105.3 °C for geothermal groundwater. However, the reservoir temperatures of four thermal springs (131.0 to 138.9 °C) estimated by the quartz geothermometer after steam loss seemed to be more in line with the actual geological and geothermal background. If the maximum reservoir temperature is 138.9 °C, it only requires 453 kJ/kg energy to heat the groundwater, thus indicating low enthalpy in the geothermal system.

5.2. Origin of the groundwater

H and O stable isotopes of groundwater are powerful geochemical tools to determine the origin, nature, distribution and water–rock interactions of fluids in geothermal systems, after modification by

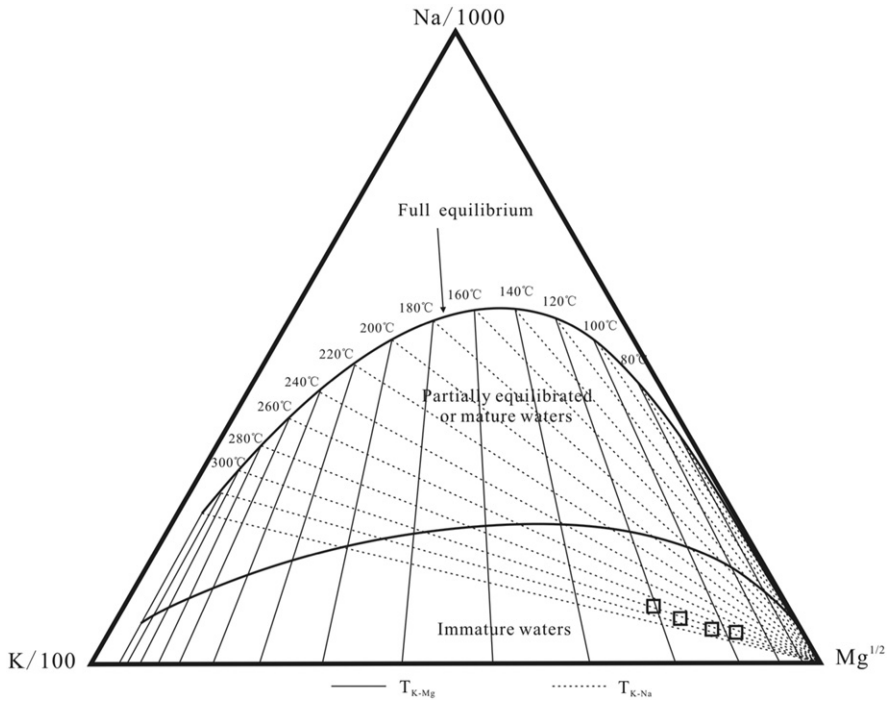

Fig. 4. Distribution of thermal springs from Dongguan Basin of Southern China in the modified Na/400–K/100–$Mg^{1/2}$ (in mg/L) ternary diagram after Giggenbach (1988) and Shevenell and Goff (1995). T_{K-Mg} and T_{K-Na} represent the K–Mg apparent temperatures and K–Na apparent temperatures, respectively.

evaporation and mixing in shallow aquifers and by isotopic exchange with minerals (Capasso et al., 1992; Caprarelli et al., 1997; Pang, 2006; Pichler, 2005; Simmons et al., 1994; Tole, 1990). The relationships of δD and $\delta^{18}O$ for thermal and non-thermal groundwater from Dongguan Basin were illustrated in Fig. 7 together with the global and regional meteoric water lines and the local river water and rain water. Thermal spring water and non-thermal spring water are almost identical and closely focused at the global meteoric water line (GMWL) in Fig. 7. And all the well waters also are close to GMWL as well as the river water. But rain water and borehole water (DG-15) are closely located at the regional meteoric water line (RMWL). Therefore, all the thermal and non-thermal water are basically considered to be meteoric origin.

Temperature and meteoric water isotopes were monitored in Dongguan city and other four cities of Guangdong province from 2013 to 2014. According to the monitoring data in summer season in Dongguan City, the average temperature is 30.5 °C, and δD and $\delta^{18}O$ of meteoric water are −43.2‰ and −6.83‰, respectively. The rain water collected in October at about 20 °C of atmospheric temperature had more negative isotopic compositions than those of other water samples, indicating that groundwater was recharged by meteoric water in summer at higher atmospheric temperature. Although the borehole (DG-12), located at the estuary shore of Pearl River in the center of Dongguan Basin, had the maximum values of isotopic compositions. It is still close to RMWL with the highest salinity, indicating that the isotopic compositions of H and O changed scarcely for the isotope exchange of groundwater-gypsum salt minerals. Consequently, it is

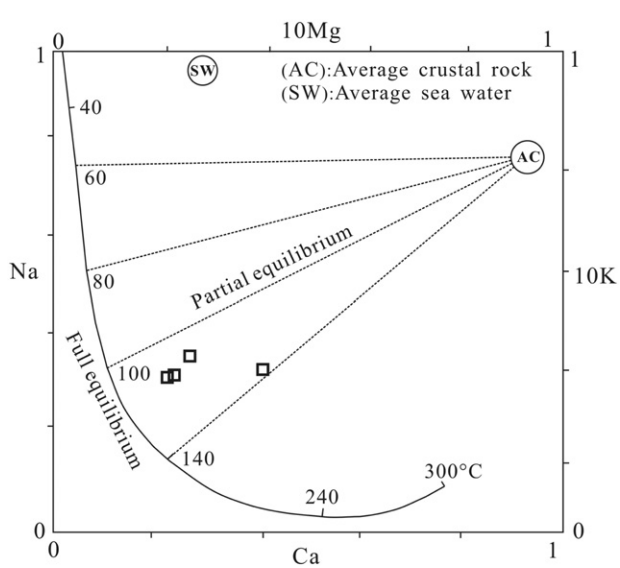

Fig. 5. Plot of $10C_{Mg}/(10C_{Mg} + C_{Ca})$ versus $10C_K/(10C_K + C_{Ca})$ of the studied thermal springs (C_i in mg/kg).

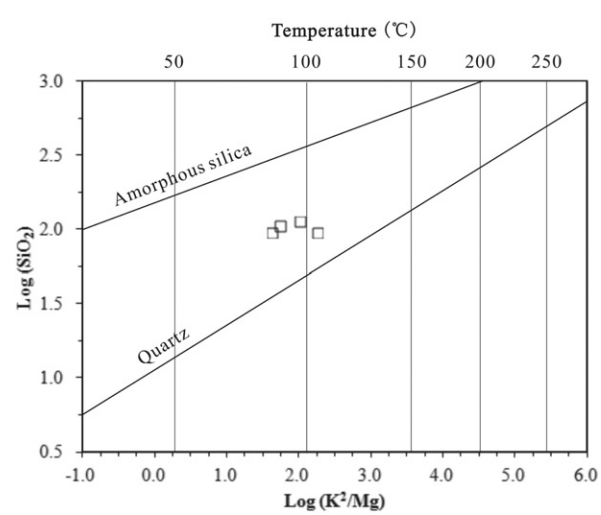

Fig. 6. A plot of log SiO_2 against the logarithm of the K^2/Mg ratio for thermal springs from Dongguan Basin of Southern China on amorphous silica and quartz geothermometer equations (Giggenbach, 1988; Giggenbach and Glovert, 1992).

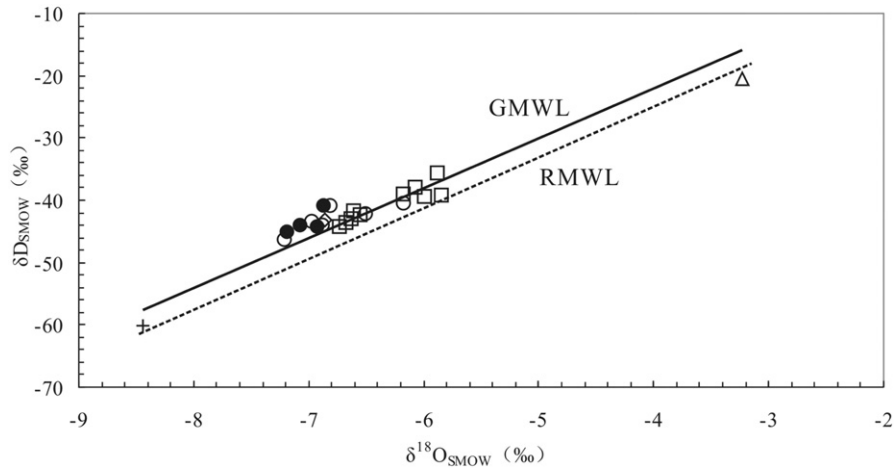

Fig. 7. Relationships of δD and $\delta^{18}O$ for thermal and non-thermal water from Dongguan Basin of Southern China. The straight line ($\delta D = 8.0\delta^{18}O + 10.0$) represents the global meteoric water line (GMWL), and the dotted line ($\delta D = 8.2\delta^{18}O + 7.8$) represents the regional meteoric water line (RMWL); the dots represent the thermal springs, the circles represent the non-thermal spring, the squares the represent wells, the triangle represents the borehole (DG-12), the prismatic represents the river water, and the cross represents the rain.

presumed that the isotopic compositions of all water samples are mainly associated with recharging temperature because their geographic discrepancies are almost negligible. The thermal springs are much close to non-thermal springs and most of wells in Fig. 7, indicating they have consistent recharge temperature. Therefore, the thermal springs were recharged at about 25 °C according to the average temperature of non-thermal springs and wells.

5.3. Mechanism of the thermal springs

The hydrogeochemical and stable isotopic characteristics of thermal and non-thermal groundwater from Dongguan Basin of Southern China helped to outline the mechanism of thermal springs. The remarkable similarities of hydrogeochemical and stable isotopic compositions for thermal springs and non-thermal springs and wells indicate similar sources of both water types. And meteoric water was regarded as the regional groundwater recharge and supplied the thermal and non-thermal springs.

Various geothermometers were applied to explore the deep reservoir temperatures for the thermal springs, and the temperatures estimated by the quartz geothermometer after steam loss (131.0 to 138.9 °C) was regarded as the most possibility. Saturation index (SI) of thermodynamic mineral equilibrium can give an insight into the groundwater rock interaction at high temperature (Chandrajith et al., 2013; Mohammadi et al., 2010). The results were calculated with the computer code PHREEQC v. 3.0.6–7757, and listed in Table 4. Except quartz, almost all the calculated minerals were unsaturated in thermal springs and non-thermal springs and wells for SI < 0, indicating inadequate equilibrium between water and rock interaction. With respect to each calculated mineral, the saturation of thermal springs was slightly higher than that of non-thermal springs and wells. The results suggested that similar groundwater–rock interactions possibly occurred in the formation of thermal and non-thermal springs. As to silica in

Table 4
Saturation index (SI) calculations of thermal and non-thermal springs from Dongguan Basin of Southern China using PHREEQC v. 3.0.6-7757.

	Anhydrite	Aragonite	Calcite	Chalcedony	Chrysotile	CO_2 (g)	Dolomite	Fluorite	Gypsum	Halite	Quartz	Sepiolite	Sepiolite (d)	SiO_2 (a)	Sylvite	Talc
DG-01	−2.90	−3.61	−3.47	−0.16	−16.94	−1.97	−7.41	−1.51	−2.59	−8.22	0.27	−11.76	−14.65	−1.00	−7.86	−13.56
DG-02	−3.96	−3.86	−3.71	−0.15	−17.92	−1.79	−7.79	−3.30	−3.65	−8.81	0.28	−12.38	−15.27	−0.99	−8.59	−14.53
DG-03	−4.30	−2.07	−1.92	−0.09	−8.38	−3.10	−4.16	−3.60	−3.99	−9.04	0.35	−5.90	−8.78	−0.93	−9.44	−4.87
DG-04	−3.69	−2.53	−2.39	−0.11	−15.34	−1.50	−5.34	−2.00	−3.38	−8.44	0.33	−10.58	−13.46	−0.95	−8.34	−11.86
DG-05	−2.98	−2.32	−2.18	−0.11	−15.19	−1.33	−4.94	−2.76	−2.68	−7.49	0.32	−10.53	−13.44	−0.95	−7.22	−11.71
DG-06	−3.20	−3.27	−3.13	−0.42	−18.93	−1.04	−6.65	−2.28	−2.90	−7.61	0.01	−13.55	−16.47	−1.26	−7.42	−16.06
DG-07	−3.28	−2.04	−1.89	−0.18	−10.02	−2.39	−3.91	−2.44	−2.97	−8.45	0.25	−7.16	−10.04	−1.03	−8.36	−6.69
DG-08	−3.75	−2.73	−2.58	−0.64	−18.23	−1.32	−6.00	–	−3.45	−8.48	−0.21	−13.45	−16.36	−1.48	−8.92	−15.81
DG-09	−3.59	−2.85	−2.71	−0.18	−16.27	−1.21	−5.66	−1.89	−3.29	−8.25	0.25	−11.37	−14.28	−1.02	−8.39	−12.93
DG-10	−4.60	−3.48	−3.33	−0.10	−17.01	−1.53	−6.81	−3.83	−4.26	−9.23	0.34	−11.62	−14.44	−0.95	−9.10	−13.55
DG-11	−4.29	−2.53	−2.39	−0.28	−12.00	−2.51	−5.12	−3.16	−3.98	−9.22	0.15	−8.66	−11.53	−1.13	−8.98	−8.89
DG-12	−0.62	0.36	0.50	−0.13	−2.21	−2.29	1.08	–	−0.34	−3.14	0.30	−1.97	−4.92	−0.96	−4.19	1.26
DG-13	−2.49	−0.17	−0.05	0.06	−6.04	−1.24	−1.05	0.10	−2.57	−7.60	0.38	−5.40	−9.19	−0.66	−8.72	−1.79
DG-14	−2.12	−0.19	−0.06	0.17	−6.09	−1.52	−1.19	0.19	−2.14	−7.25	0.51	−5.06	−8.71	−0.58	−8.40	−1.69
DG-15	−3.50	0.17	0.28	−1.03	8.64	−6.13	−0.59	−0.50	−3.72	−7.33	−0.75	2.12	−1.97	−1.72	−8.60	10.84
DG-16	−2.63	0.01	0.13	0.16	−4.25	−1.79	−0.76	0.25	−2.68	−7.27	0.49	−3.94	−7.66	−0.57	−8.44	0.17
DG-17	−3.10	−0.27	−0.13	0.25	−8.47	−1.90	−1.44	−0.36	−2.79	−8.65	0.68	−5.43	−8.33	−0.59	−8.76	−4.27
DG-18	−3.37	−2.64	−2.49	−0.26	−15.60	−1.32	−5.25	−2.21	−3.06	−8.32	0.17	−11.01	−13.89	−1.10	−8.41	−12.42
DG-19	−3.59	−2.00	−1.86	−0.34	−12.19	−1.96	−4.11	−2.91	−3.29	−9.08	0.09	−8.93	−11.84	−1.18	−8.96	−9.15
DG-20	−1.85	−0.12	0.02	−0.28	−8.42	−1.55	−0.68	−1.40	−1.59	−7.43	0.14	−6.42	−9.41	−1.11	−7.24	−5.24
DG-21	−2.59	−2.41	−2.27	−0.33	−16.51	−0.98	−4.97	−2.55	−2.29	−7.55	0.10	−11.78	−14.69	−1.17	−7.56	−13.46
DG-22	−4.68	−3.56	−3.42	−0.14	−15.73	−1.69	−6.64	−4.08	−4.35	−9.25	0.30	−10.86	−13.70	−0.99	−9.00	−12.34

–, not calculated.

most of thermal and non-thermal springs and wells, quartz was slightly saturated, possibly due to conductive cooling; whereas chalcedony and amorphous silica were slightly under-saturated and close to the equilibrium, possibly due to rapid cooling (Table 4). The quartz equilibrium can be achieved at temperatures as low as 70 °C whereas below that the equilibrium with chalcedony will control the dissolution of silica (Fournier and Truesdell, 1970; Mariner et al., 1993; Mohammadi et al., 2010). Thermal springs had quartz and chalcedony near and slightly above the saturation limit for equilibrium, indicating that the original silica content was preserved and did not re-equilibrate during circulation. It is possibly due to faster circulation in a relatively fast conductive fracture system hosted by deep-seated faults in Dongguan Basian of Southern China. And the total dissolved solid (TDS, 276–326 mg/L) in the four thermal springs is relatively low, further indicating the fast movement and disequilibrium for the geothermal groundwater.

The origin of thermal groundwater was most likely from meteoric water and circulated in crystalline rocks to different depths according to the hydrogeochemical and stable isotopic characteristics. And the close scattering of isotopic data around meteoric water lines indicated that meteoric water recharged the springs without significant evaporation prior to the infiltration. Therefore, the regional meteoric water infiltration was fast and the evaporation had neglected influence on the isotopic composition for recharge water. However, isotope exchange of water–rock can cause significant change for $\delta^{18}O$ besides evaporation, resulting in "Oxygen drift" because minerals have relatively positive values than thermal groundwater (Capaccioni et al., 2011; Panichi and Volpi, 1999; Pichler, 2005; Smith and Suemnicht, 1991). The four thermal springs, recharged at about 25 °C, had experienced temperatures over 100 °C before outcropping at the temperature of 59.8 to 78.6 °C, suggesting that the groundwater should have completed the water–rock isotopic exchange before outcropping. Consequently, "Oxygen drift" was expected to occur to the four thermal springs, meaning that the data points (black dots in Fig. 5) of four thermal springs should lie below GMWL.

However, the expected "Oxygen drift" was not observed and the data points of four thermal springs were still very close to GMWL in Fig. 5. This finding had a few implications. First, the contribution of aqueous geothermal fluids from deep-seated faults to the thermal springs must be negligible; otherwise the "Oxygen drift" is inevitable in Fig. 7 because aqueous geothermal fluids always have more positive Oxygen isotope composition (Ayuso et al., 1998; Capaccioni et al., 2011; Downes et al., 2001; Ellam and Harmon, 1990; Jung and Hoernes, 2000). Second, the thermal springs are most likely to be shallow groundwater, mixing with non-aqueous geothermal fluids (such as gas) from deep-seated faults. Third, the mixing process of shallow groundwater and non-aqueous geothermal fluids happens very rapidly because water–rock isotope exchange had not been observed yet (Bolognesi, 2011).

6. Conclusions

Conventional groundwater geochemistry together with isotope data was successfully applied to constrain the evolution of geothermal springs hosted by deep-seated faults in Dongguan Basin, Southern China. Except higher temperature and TDS as well as lower Cl- and Ca^{2+} content, thermal springs were hydrogeochemically and isotopically similar in composition to non-thermal springs and wells. Water chemical geothermometers were used to estimate the reservoir temperature and the reasonable temperature estimated by the quartz geothermometer after steam loss were 131.0 to 138.9 °C. Stable isotope data suggested that the origin of both thermal and non-thermal groundwater recharge was almost all exclusively meteoric water. The chemical and isotopic results of groundwater–rock interaction also indicated that the best suitable mechanism of thermal springs was groundwater migrating and being heated very quickly in a relatively fast conductive fracture system hosted by deep-seated faults in Dongguan Basian of Southern China.

Acknowledgments

This research project was financially supported jointly by the National Natural Science foundation of China (Grant Nos. 40602031, 41440027), Fundamental Research Funds for the Central Universities (Grant No. CUGL090213), Nature Science Foundation of Hubei Province (Grant No. 2011045003), and China Geological Survey project (Grant No. 1212011220014).

References

Arnórsson, S., 1985. The use of mixing models and chemical geothermometers for estimating underground temperatures in geothermal systems. J. Volcanol. Geotherm. Res. 23, 299–335.
Arnórsson, S., Gunnlaugsson, E., Svavarsson, H., 1983. The chemistry of geothermal waters in Iceland. III. Chemical geothermometry in geothermal investigations. Geochim. Cosmochim. Acta 47, 567–577.
Ayuso, R.A., De Vivo, B., Rolandi, G., Seal Ii, R.R., Paone, A., 1998. Geochemical and isotopic (Nd–Pb–Sr–O) variations bearing on the genesis of volcanic rocks from Vesuvius, Italy. J. Volcanol. Geotherm. Res. 82, 53–78.
Ben Dhia, H., Meddeb, N., 1990. Application of chemical geothermometers to some Tunisian hot springs. Geothermics 19, 87–104.
Bolognesi, L., 2011. The oxygen isotope exchange between carbon dioxide and water in the Larderello geothermal field (Italy) during fluid reinjection. Geothermics 40, 181–189.
Capaccioni, B., Vaselli, O., Tassi, F., Santo, A.P., Huertas, A.D., 2011. Hydrogeochemistry of the thermal waters from the Sciacca Geothermal Field (Sicily, southern Italy). J. Hydrol. 396, 292–301.
Capasso, G., Dongarrà, G., Favara, R., Hauser, S., Valenza, M., 1992. Isotope composition of rain water, well water and fumarole steam on the island of Vulcano, and their implications for volcanic surveillance. J. Volcanol. Geotherm. Res. 49, 147–155.
Caprarelli, G., Tsutsumi, M., Turi, B., 1997. Chemical and isotopic signatures of the basement rocks from the Campi Flegrei geothermal field (Naples, southern Italy): inferences about the origin and evolution of its hydrothermal fluids. J. Volcanol. Geotherm. Res. 76, 63–82.
Chandrajith, R., Barth, J.A.C., Subasinghe, N.D., Merten, D., Dissanayake, C.B., 2013. Geochemical and isotope characterization of geothermal spring waters in Sri Lanka: evidence for steeper than expected geothermal gradients. J. Hydrol. 476, 360–369.
De Filippis, L., Billi, A., 2012. Morphotectonics of fissure ridge travertines from geothermal areas of Mammoth Hot Springs (Wyoming) and Bridgeport (California). Tectonophysics 548–549, 34–48.
Downes, H., Thirlwall, M.F., Trayhorn, S.C., 2001. Miocene subduction-related magmatism in southern Sardinia: Sr–Nd- and oxygen isotopic evidence for mantle source enrichment. J. Volcanol. Geotherm. Res. 106, 1–22.
Du, J., Liu, C., Fu, B., Ninomiya, Y., Zhang, Y., Wang, C., Wang, H., Sun, Z., 2005. Variations of geothermometry and chemical-isotopic compositions of hot spring fluids in the Rehai geothermal field, southwestern China. J. Volcanol. Geotherm. Res. 142, 243–261.
Duchi, V., Minissale, A., Paolieri, M., Prati, F., Valori, A., 1992. Chemical relationship between discharging fluids in the Siena-Radicofani graben and the deep fluids produced by the geothermal fields of Mt Amiata, Torre Alfina and Latera (Central Italy). Geothermics 21, 401–413.
Dulanya, Z., Morales-Simfors, N., Sivertun, Å., 2010. Comparative study of the silica and cation geothermometry of the Malawi hot springs: potential alternative energy source. J. Afr. Earth Sci. 57, 321–327.
Ellam, R.M., Harmon, R.S., 1990. Oxygen isotope constraints on the crustal contribution to the subduction-related magmatism of the Aeolian Islands, southern Italy. J. Volcanol. Geotherm. Res. 44, 105–122.
Fischer, T.P., Sturchio, N.C., Stix, J., Arehart, G.B., Counce, D., Williams, S.N., 1997. The chemical and isotopic composition of fumarolic gases and spring discharges from Galeras Volcano, Colombia. J. Volcanol. Geotherm. Res. 77, 229–253.
Fournier, R.O., 1977. Estimates of temperatures and salinities of aquifers in geothermal system at Cerro-Prieto, Mexico from hot-spring data. Econ. Geol. 72, 728–738.
Fournier, R.O., Potter Ii, R.W., 1979. Magnesium correction to the Na–K–Ca chemical geothermometer. Geochim. Cosmochim. Acta 43, 1543–1550.
Fournier, R.O., Truesdell, A.H., 1970. Chemical indicators of subsurface temperature applied to hot spring waters of Yellowstone National Park, Wyoming, U.S.A. Geothermics 2 (Part 1), 529–535.
Fournier, R.O., Truesdell, A.H., 1973. An empirical Na–K–Ca geothermometer for natural waters. Geochim. Cosmochim. Acta 37, 1255–1275.
GBGMI, 1988. Local Chronicles of the Regional Geology in Guangdong Province. Guangdong Bureau of Geology and Mineral Investigation, pp. 10–830 (in Chinese with English abstract).
Giggenbach, W.F., 1988. Geothermal solute equilibria. Derivation of Na–K–Mg–Ca geoindicators. Geochim. Cosmochim. Acta 52, 2749–2765.
Giggenbach, W.F., Glovert, R.B., 1992. Tectonic regime and major processes governing the chemistry of water and gas discharges from the Rotorua geothermal field, New Zealand. Geothermics 21, 121–140.

Guido, D.M., Campbell, K.A., 2012. Diverse subaerial and sublacustrine hot spring settings of the Cerro Negro epithermal system (Jurassic, Deseado Massif), Patagonia, Argentina. J. Volcanol. Geotherm. Res. 229–230, 1–12.
Guo, Q., Wang, Y., 2012. Geochemistry of hot springs in the Tengchong hydrothermal areas, Southwestern China. J. Volcanol. Geotherm. Res. 215–216, 61–73.
Guo, F., Fan, W.M., Li, C.W., Zhao, L., Li, H.X., Yang, J.H., 2012. Multi-stage crust–mantle interaction in SE China: temporal, thermal and compositional constraints from the Mesozoic felsic volcanic rocks in eastern Guangdong–Fujian provinces. Lithos 150, 62–84.
Han, Y., Huh, Y., 2009. A geochemical reconnaissance of the Duman (Tumen) River and the hot springs of Mt. Baekdu (Changbai): weathering of volcanic rocks in mid-latitude setting. Chem. Geol. 264, 162–172.
Huang, H.F., Goff, F., 1986. Hydrogeochemistry and reservoir model of Fuzhou geothermal field, China. J. Volcanol. Geotherm. Res. 27, 203–227.
Ishikawa, H., Ohba, T., Fujimaki, H., 2007. Sr isotope diversity of hot spring and volcanic lake waters from Zao volcano, Japan. J. Volcanol. Geotherm. Res. 166, 7–16.
Jung, S., Hoernes, S., 2000. The major- and trace-element and isotope (Sr, Nd, O) geochemistry of Cenozoic alkaline rift-type volcanic rocks from the Rhön area (central Germany): petrology, mantle source characteristics and implications for asthenosphere–lithosphere interactions. J. Volcanol. Geotherm. Res. 99, 27–53.
Larson, P.B., Phillips, A., John, D., Cosca, M., Pritchard, C., Andersen, A., Manion, J., 2009. A preliminary study of older hot spring alteration in Sevenmile Hole, Grand Canyon of the Yellowstone River, Yellowstone Caldera, Wyoming. J. Volcanol. Geotherm. Res. 188, 225–236.
Lau, C.Y., Aitchison, J.C., Pointing, S.B., 2008. Early colonization of thermal niches in a silica-depositing hot spring in central Tibet. Geobiology 6, 136–146.
Liang, H.Y., Xia, P., Wang, X.Z., Cheng, J.P., Zhao, Z.H., Liu, C.Q., 2007. Geology and geochemistry of the adjacent Changkeng gold and Fuwang silver deposits, Guangdong Province, South China. Ore Geol. Rev. 31, 304–318.
Lin, L., Pang, Y.C., Ma, L.Y., Yang, Y.J., Li, D.L., 2010. Submarine hydrothermal/hot spring deposition of Early Cambrian Niutitang Formation in South China. J. Earth Sci-China 21, 40–43.
Majumdar, N., Majumdar, R.K., Mukherjee, A.L., Bhattacharya, S.K., Jani, R.A., 2005. Seasonal variations in the isotopes of oxygen and hydrogen in geothermal waters from Bakreswar and Tantloi, Eastern India: implications for groundwater characterization. J. Asian Earth Sci. 25, 269–278.
Mariner, R.H., Presser, T.S., Evans, W.C., 1993. Geothermometry and water–rock interaction in selected thermal systems in the cascade range and modoc plateau, western United States. Geothermics 22, 1–15.
Minissale, A., Magro, G., Vaselli, O., Verrucchi, C., Perticone, I., 1997. Geochemistry of water and gas discharges from the Mt. Amiata silicic complex and surrounding areas (central Italy). J. Volcanol. Geotherm. Res. 79, 223–251.
Minissale, A., Chandrasekharam, D., Vaselli, O., Magro, G., Tassi, F., Pansini, G.L., Bhramhabut, A., 2003. Geochemistry, geothermics and relationship to active tectonics of Gujarat and Rajasthan thermal discharges, India. J. Volcanol. Geotherm. Res. 127, 19–32.
Minissale, A., Mattash, M.A., Vaselli, O., Tassi, F., Al-Ganad, I.N., Selmo, E., Shawki, N.M., Tedesco, D., Poreda, R., Ad-Dukhain, A.M., Hazzae, M.K., 2007. Thermal springs, fumaroles and gas vents of continental Yemen: their relation with active tectonics, regional hydrology and the country's geothermal potential. Appl. Geochem. 22, 799–820.
Mohammadi, Z., Bagheri, R., Jahanshahi, R., 2010. Hydrogeochemistry and geothermometry of Changal thermal springs, Zagros region, Iran. Geothermics 39, 242–249.
Mottl, M.J., Seewald, J.S., Wheat, C.G., Tivey, M.K., Michael, P.J., Proskurowski, G., McCollom, T.M., Reeves, E., Sharkey, J., You, C.F., Chan, L.H., Pichler, T., 2011. Chemistry of hot springs along the Eastern Lau Spreading Center. Geochim. Cosmochim. Acta 75, 1013–1038.
Pang, Z., 2006. pH dependant isotope variations in arc-type geothermal waters: new insights into their origins. J. Geochem. Explor. 89, 306–308.
Panichi, C., Volpi, G., 1999. Hydrogen, oxygen and carbon isotope ratios of Solfatara fumaroles (Phlegrean Fields, Italy): further insight into source processes. J. Volcanol. Geotherm. Res. 91, 321–328.
Parkhurst, D.L., Appelo, C.A.J., 2013. Description of Input and Examples for PHREEQC Version 3—A Computer Program for Speciation, Batch-reaction, One-dimensional transport, and Inverse Geochemical Calculations: U.S. Geological Survey Techniques and Methods, Book 6, chap. A43. (497 pp., available only at http://pubs.usgs.gov/tm/06/a43/).
Parry, W.T., Bowman, J.R., 1990. Chemical and stable isotopic models for boundary creek warm springs, southwestern Yellowstone National Park, Wyoming. J. Volcanol. Geotherm. Res. 43, 133–157.
Pauwels, H., Fouillac, C., Fouillac, A.-M., 1993. Chemistry and isotopes of deep geothermal saline fluids in the Upper Rhine Graben: origin of compounds and water–rock interactions. Geochim. Cosmochim. Acta 57, 2737–2749.
Pichler, T., 2005. Stable and radiogenic isotopes as tracers for the origin, mixing and subsurface history of fluids in submarine shallow-water hydrothermal systems. J. Volcanol. Geotherm. Res. 139, 211–226.
Pope, L.A., Hajash, A., Popp, R.K., 1987. An experimental investigation of the quartz, Na–K, Na–K–Ca geothermometers and the effects of fluid composition. J. Volcanol. Geotherm. Res. 31, 151–161.
Ruffa, G.L., Panichi, C., Kavouridis, T., Liberopoulou, V., Leontiadis, J., Caprai, A., 1999. Isotope and chemical assessment of geothermal potential of Kos Island, Greece. Geothermics 28, 205–217.
Shevenell, L., Goff, F., 1995. Evolution of hydrothermal waters at Mount St. Helens, Washington, USA. J. Volcanol. Geotherm. Res. 69, 73–94.
Simmons, S.F., Stewart, M.K., Robinson, B.W., Glover, R.B., 1994. The chemical and isotopic compositions of thermal waters at Waimangu, New Zealand. Geothermics 23, 539–553.
Smith, B.M., Suemnicht, G.A., 1991. Oxygen isotope evidence for past and present hydrothermal regimes of Long Valley caldera, California. J. Volcanol. Geotherm. Res. 48, 319–339.
Song, G., Wang, X., Chen, D., Chen, Y., 2011. Contribution of ^{222}Rn-bearing water to indoor radon and indoor air quality assessment in hot spring hotels of Guangdong, China. J. Environ. Radioact. 102, 400–406.
Spycher, N., Peiffer, L., Sonnenthal, E.L., Saldi, G., Reed, M.H., Kennedy, B.M., 2014. Integrated multicomponent solute geothermometry. Geothermics 51, 113–123.
Sun, Z.X., Gao, B., Zhang, Z.S., 2006. Geochemistry of geothermal fluids from the Maanping Hotspring Area, Jiangxi Province, SE-China. Geochim. Cosmochim. Acta 70, A630.
Tassi, F., Vaselli, O., Capaccioni, B., Macias, J.L., Nencetti, A., Montegrossi, G., Magro, G., 2003. Chemical composition of fumarolic gases and spring discharges from El Chichòn volcano, Mexico: causes and implications of the changes detected over the period 1998–2000. J. Volcanol. Geotherm. Res. 123, 105–121.
Thiebaud, E., Dzikowski, M., Gasquet, D., Renac, C., 2010. Reconstruction of groundwater flows and chemical water evolution in an amagmatic hydrothermal system (La Lechere, French Alps). J. Hydrol. 381, 189–202.
Tole, M.P., 1990. Stable isotope studies of some low enthalpy geothermal systems in Kenya. J. Afr. Earth Sci. 11, 33–37 (and the Middle East).
Ueda, A., Shimoda, S., Nagao, K., Shibata, T., Suzuki, T., 2006. Stable and noble gas isotopic study of geothermal and ground waters in North Hokkaido, Japan. Geochim. Cosmochim. Acta 70, A678-A678.
Verma, M.P., 2000. Chemical thermodynamics of silica: a critique on its geothermometer. Geothermics 29, 323–346.
Verma, M.P., 2008. Qrtzgeotherm: an ActiveX component for the quartz solubility geothermometer. Comput. Geosci. 34, 1918–1925.
Verma, S.P., Santoyo, E., 1997. New improved equations for Na/K, Na/Li and SiO_2 geothermometers by outlier detection and rejection. J. Volcanol. Geotherm. Res. 79, 9–23.
Werner, C., Hurwitz, S., Evans, W.C., Lowenstern, J.B., Bergfeld, D., Heasler, H., Jaworowski, C., Hunt, A., 2008. Volatile emissions and gas geochemistry of Hot Spring Basin, Yellowstone National Park, USA. J. Volcanol. Geotherm. Res. 178, 751–762.
Ye, L., Liu, T.G., Yang, Y.L., Gao, W., Pan, Z.P., Bao, T., 2014. Petrogenesis of bismuth minerals in the Dabaoshan Pb-Zn polymetallic massive sulfide deposit, northern Guangdong Province, China. J. Asian Earth Sci. 82, 1–9.
Yokoyama, T., Nakai, S.i., Wakita, H., 1999. Helium and carbon isotopic compositions of hot spring gases in the Tibetan Plateau. J. Volcanol. Geotherm. Res. 88, 99–107.
Zaher, M.A., Saibi, H., Nishijima, J., Fujimitsu, Y., Mesbah, H., Ehara, S., 2012. Exploration and assessment of the geothermal resources in the Hammam Faraun hot spring, Sinai Peninsula. Egypt. J. Asian Earth Sci. 45, 256–267.
Zhou, X., Fang, B., Zhou, H.Y., Li, J., Wang, Y., 2009. Isotopes of deuterium and oxygen-18 in thermal groundwater in China. Environ. Geol. 57, 1807–1814.
Zhu, W.G., Zhong, H., Li, X.H., He, D.F., Song, X.Y., Ren, T., Chen, Z.Q., Sun, H.S., Liao, J.Q., 2010. The Early Jurassic mafic–ultramafic intrusion and A-type granite from northeastern Guangdong, SE China: age, origin, and tectonic significance. Lithos 119, 313–329.